Soft Matter

PAPER

View Article Online
View Journal | View Issue



Cite this: *Soft Matter*, 2014, **10**, 8464

# Phase diagram of inverse patchy colloids assembling into an equilibrium laminar phase

Eva G. Noya,*[a] Ismene Kolovos,[b] Günther Doppelbauer,[b] Gerhard Kahl[b] and Emanuela Bianchi[b]

Received 15th July 2014
Accepted 27th August 2014

DOI: 10.1039/c4sm01559b

www.rsc.org/softmatter

We numerically study the phase behavior of colloidal particles with two charged patches at the poles and an oppositely charged equatorial belt. Interactions between particles are described using the inverse patchy colloid model, where the term *inverse* emphasizes the difference with respect to conventional patchy particles: as a consequence of the heterogeneous charge distribution, the patches on the particle surface repel each other, whereas the patches and non-patch regions mutually attract. For the model parameters considered in this work, the system exhibits an unusual equilibrium phase diagram characterized by a broad region where a novel structure composed of parallel colloidal monolayers is stable.



## I. Introduction

In the last few years the theoretical investigation of the phase behavior of particles with anisotropic shapes and/or interactions has been a very active field of research.[1–3] The study of these particles is not only interesting from a fundamental point of view but is also motivated by the advances in colloidal science that allow the synthesis of exotic building blocks for the self-assembly of new materials.[2,4,5] Anisotropically interacting particles can exhibit an amazingly rich and unusual phase behavior[6–9] and they are thus nowadays regarded as ideal building blocks of novel self-assembled materials with specific symmetries and physical properties.[1]

In this paper, we consider colloidal particles whose anisotropic interactions originate from the presence of differently charged surface regions. These particles have been presented in ref. 10 and are referred to as inverse patchy colloids (IPCs). In contrast to conventional patchy colloids,[3] IPCs are mutually repulsive particles carrying extended patches that repel each other and attract those parts of the colloid that are free of patches; these systems are thus characterized by a non-trivial interplay between attractive and repulsive directional interactions. IPCs can be considered as representatives of a wide class of inhomogeneously charged units, spanning from viral capsids to virus-like nanoparticles and spotted vesicles.[11–13] Within this broad class of systems, we focus on heterogeneously charged aggregates that feature one of the simplest possible surface patterns: we consider spherical particles decorated by two polar patches and an oppositely charged equatorial belt.

Investigations of IPCs under planar confinement have shown a wealth of different assemblies with tunable spatial and orientational order,[14,15] the formation of quasi two-dimensional aggregates being an emergent feature under these confinement conditions:[14,15] as soon as more than two particles are involved, IPCs bond to their neighbors with their symmetry axes oriented in plane, thus favoring the formation of monolayers; within these colloidal layers the bare equatorial regions of the particles are exposed, so that a growth along the direction perpendicular to the planar assembly is disfavored.

In this contribution we select an IPC system prone to form planar aggregates in the bulk and we study its equilibrium phase diagram. Our particular interest in the formation and stability of two-dimensional colloidal sheets is driven by the wealth of direct applications for optoelectronic and data storage devices; lamellar structures have indeed outstanding mechanical and optical properties, such as an enhanced photoconductivity response or a phenomenal external load stability.[16–18] The template-free organization of particles into planar structures has been observed in a variety of either natural or synthesized systems, such as S-layer proteins,[19] nacre-like systems,[20] or CdTe, PbS and PbSe nanoparticles.[16–18] In all the aforementioned systems, the self-assembly of the lamellar phase occurs in equilibrium and originates mainly from anisotropic interactions, *e.g.* dipolar interactions, hydrophobic attractions, and site-specific binding. Also Janus particles as well as particles with patches arranged in an *ad hoc* geometry on the particle surface have been shown to form a variety of mono/double-layer structures and wrinkled planes,[21–25] thus opening the way to theoretical investigations on the interplay between the thermodynamics and the directional nature of the particle–particle interactions.

[a]*Instituto de Química Física Rocasolano, CSIC, Calle Serrano 119, E-28006 Madrid, Spain. E-mail: eva.noya@iqfr.csic.es*

[b]*Institut für Theoretische Physik and Center for Computational Materials Science (CMS), Technische Universität Wien, Wiedner Hauptstraße 8-10, A-1040 Wien, Austria*

Here we show how one of the simplest charge distributions on the colloidal surface allows the formation of an equilibrium phase composed of parallel crystalline monolayers. More specifically, we select an IPC system which shows in its zero-temperature phase diagram the presence of an equilibrium lamellar phase and we investigate the stability of such a structure at finite temperature. Our findings highlight the potentialities of IPC systems as they result from a non-trivial interplay between attractive and repulsive directional interactions: in addition to two face-centered-cubic lattices, the phase diagram of the selected system is characterized by a quite broad region where the lamellar phase is stable.

The paper is structured as follows: section II introduces the model, its parameters and its zero-temperature phase diagram, section III describes the free energy calculations used to evaluate the finite temperature phase diagram of the selected system, section IV reports the results of our investigation, and section V summarizes our conclusive remarks. Details on the integration paths and consistency checks on the calculation of free energies and coexistence points are given in the Appendix.

## II. Model

The IPC model introduced in ref. 10 features a spherical, hard colloid of radius $\sigma$ with a surface pattern defined by two charged polar areas and one oppositely charged equatorial region. The particle diameter of $2\sigma$ sets the length unit.

The coarse-grained potential between two IPCs is given by an isotropic, hard-core repulsion, that models the steric constraint, and a direction-dependent contribution, that can be overall attractive or repulsive depending on the relative orientation of the two particles. Such a directional contribution results from the interplay between the differently charged regions on the particle surface and can be described by considering the corresponding interplay between the interaction spheres of both the bare colloids and the patches. The directional contribution to the pair potential can be factorized into three parts corresponding to the EE, EP and PP interaction types, where the letters refer to the equatorial–equatorial, equatorial–polar and polar–polar interactions. By postulating that the energy strength of each interaction type is a constant, while the relevance of each interaction is imposed by the relative geometry of the two IPCs, the directional part of the potential can be written as[10] $V = \omega_{EE}u_{EE} + \omega_{EP}u_{EP} + \omega_{PP}u_{PP}$, where the dependence on the distance and on the mutual orientation of the two particles is omitted for the sake of simplicity. In the preceding expression, $u_{EE}$, $u_{EP}$ and $u_{PP}$ are the constant energy strengths of the EE, EP and PP interactions, while $\omega_{EE}$, $\omega_{EP}$ and $\omega_{PP}$ are dimensionless weights that are proportional to the overlap volumes of the corresponding interaction spheres. While the overlap volumes for a given two particle configuration are fixed by the choice of both the interaction range and the patch size, the energy constants are set by mapping (with the so-called "max" scheme) the coarse-grained potential to the analytical Debye–Hückel potential.[10]

The resulting pair potential is characterized by three independent parameters:[10] (i) the interaction range $\delta$, that depends on the salt concentration, (ii) the surface extension of the polar caps, that is defined by the opening angle $\gamma$ (defined as half the opening angle), and (iii) the set of contact energies for three characteristic particle–particle configurations $\bar{\varepsilon}$, that is fixed by the ratio between the charge of the bare colloid $Z_c$ and the charge of the patches $Z_p$. The latter set of parameters can be written as $\bar{\varepsilon} = (\varepsilon_{PP}, \varepsilon_{EE}, \varepsilon_{EP})$ – see panel (a) of Fig. 1. The minimum of the equatorial–polar attraction, $|\varepsilon_{EP}|$, sets the energy unit.

In the present paper we consider moderately overcharged colloids under low electrostatic screening conditions. Specifically, we fix $\kappa\sigma = 2$, where $\kappa^{-1} = \delta$ is the Debye screening length; thus $\delta = 0.25$ in units of the particle diameter. We consider IPCs that are decorated with polar patches defined by $\gamma = 38.6°$ and that are characterized by the set $\bar{\varepsilon} = (1.94, 0.39, -1.00)$ in units of $\varepsilon_{EP}$ (see panel (b) of Fig. 1). The set $\bar{\varepsilon}$ results from considering real colloids of diameter $\approx 60$ nm, with a total charge $Z_{tot} = Z_c + 2Z_p = 1/11Z_c$, dispersed in water at room temperature.[10] The corresponding reference energy is $\varepsilon_{EP} = -15.71$ in units of $k_BT$.[26]

Throughout this article, all the magnitudes will be expressed in reduced units with respect to the distance and energy units, *i.e.*, the reduced temperature is $T^* = k_BT/|\varepsilon_{EP}|$ and the reduced pressure is $p^* = p(2\sigma)^3/|\varepsilon_{EP}|$.

The present set of model parameters has been selected among others on the basis of its zero-temperature phase diagram.[27] On varying the patch size and the overall particle charge, the zero-temperature phase diagram in the density–pressure plane has been evaluated for different IPC systems[27] using an optimization technique based on evolutionary algorithms which has recently proven to be very efficient and robust in predicting stable crystal phases for patchy particle models.[28,29]

For the specific model selected here, two ordered structures have been identified as global enthalpy minima (see Fig. 2). At $p^* \lesssim 1.30$, the most stable structure is a phase

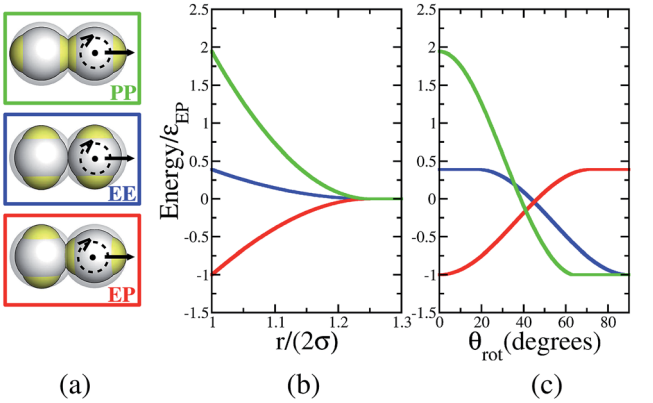


Fig. 1 Panel (a) shows three characteristic particle–particle orientations for two IPCs at contact, namely the polar–polar (PP), the equatorial–equatorial (EE) and the equatorial–polar (EP) configurations. Panels (b) and (c) show the radial and orientational dependence of the interaction between two IPCs in the three characteristic configurations: in panel (b) particles keep their mutual orientation and are separated by a distance $r$, in panel (c) particles are kept in contact and are rotated by an angle $\theta$; the green/blue/red line corresponds to a configuration where the two colloids have reciprocal orientation referred to as PP/EE/EP.

composed of parallel layers (see the top panels of Fig. 2). As also observed for a selection of IPC systems under confinement,[14,15] particles within each layer form a grain-like bonding pattern with a triangular spatial arrangement and with the polar regions pointing to approximately the middle of the center-to-center vector that joins two adjacent nearest neighbors. Since particles pertaining to the same layer are oriented with their symmetry axes in plane, they expose their bare equatorial region to the neighboring layers, thus leading to a repulsive inter-layer interaction that prevents the layers from collapsing on top of each other. The distance between the layers at each pressure results from a competition between the energy penalty and the higher packing fraction that results when the inter-layer distance is reduced. This structure has a quite low energy ($-2.29 \lesssim U^* \lesssim -2.27$) due to the large number of equatorial–polar interactions within the layers but a relatively low packing fraction ($0.545 \lesssim \eta \lesssim 0.564$). As the pressure increases, a higher packing fraction becomes more favorable, so that for pressure values $p^* \gtrsim 1.30$ a close packed solid becomes more stable than the layered structure: in this structure particles are located at the positions of a face-centred cubic (FCC) lattice and are oriented such that they maximize the number of equatorial–polar interactions (see the bottom panels of Fig. 2). The ordered FCC structure exhibits a quite high packing fraction ($\eta \approx 0.741$) but its lattice energy is higher than that of the layered structure due to the presence of a larger number of repulsive equatorial–equatorial contacts ($U^* \approx -1.98$). As observed in other patchy particle systems,[28] one expects that at sufficiently high temperatures the particles populating the FCC lattice will have enough kinetic energy to rotate almost freely in space, thus forming a plastic crystal.

The identification of the layered structure in the *zero*-temperature phase diagram motivated us to investigate the phase behavior of such an interesting structure at *finite* temperature.

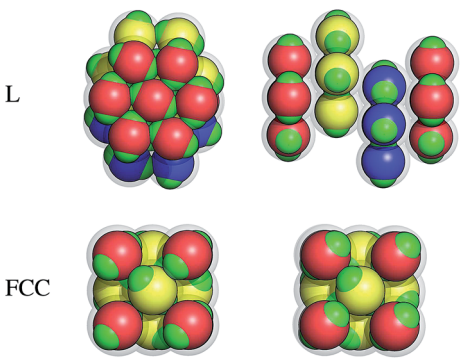


Fig. 2 Significant portions of the two structures identified as global enthalpy minima of our system by the evolutionary algorithm approach:[27] the parallel layers (L) stable for $p^* \lesssim 1.30$, and the face centered cubic crystal (FCC) stable for $p^* \gtrsim 1.30$. The colloidal cores are arbitrarily colored in red, yellow or blue to help visualization. It is worth noting that IPCs are spheres: the green caps only feature the interaction sphere of the bare patches, whose centers are located inside the colloid. The semi-transparent corona indicates the interaction sphere of the central colloid.

# III. Methods

## A. Simulation details

For the fluid phase we performed Monte Carlo (MC) simulations in the *NpT* ensemble, $N = 500$ being the number of particles in the system. Typically simulations consisted of about 200 000 MC cycles for equilibration plus another one million cycles for taking averages, where one MC cycle is defined as $N$ displacement or rotation attempts plus one volume change attempt.

For ordered structures it is important to perform anisotropic Parrinello–Rahman-like *NpT* simulations,[30,31] in which, not only the volume, but also the moduli and the angles of the vectors of the simulation box are allowed to vary independently, so that the ordered lattice can relax to its equilibrium structure, guaranteeing that the system is not under stress.[32] Simulations of the ordered structures typically extended over about 100 000 MC cycles for equilibration plus about 400 000–500 000 for taking averages. We considered $N = 500$ particles for the FCC-like ordered structure and the FCC plastic crystal, and $N = 480$ particles for the layered structure. The initial configurations of the ordered structures were generated by replicating the unit cell obtained by the optimization method mentioned before along the three spacial dimensions.

## B. Einstein molecule method

The free energy of the solid phases was evaluated using the Einstein molecule approach[32,33] which is closely related to the Einstein crystal method.[34,35] In both approaches the free energy of a given solid is calculated by designing an integration path from the real system to an Einstein crystal with the same structure as the real solid and for which the free energy can be calculated analytically or numerically.[34–32] In the Einstein crystal method the center of mass of the ensemble is kept fixed in order to avoid a quasi-divergence in the integration from the solid to the Einstein crystal, whereas in the Einstein molecule approach this is achieved by fixing the position of one molecule.[33,34] In the Einstein molecule method the translational reference field is simply given by:

$$U_{\mathrm{Ein,t}} = \sum_{i=2}^{N} \lambda_{\mathrm{t}} (\mathbf{r}_i - \mathbf{r}_{0,i})^2 \quad (1)$$

where $\lambda_{\mathrm{t}}$ is the spring constant, $\mathbf{r}_{0,i}$ is the lattice position of particle $i$ and $\mathbf{r}_i$ corresponds to its actual position.

As we are dealing with orientationally dependent interactions, the system is also coupled to an orientational field that keeps the particles in their equilibrium orientation. As shown previously,[36–38] it is useful to choose an orientational field that is characterized by the same symmetry as the particles. Since the IPCs considered in this work have axial symmetry, we used the following orientational field:

$$U_{\mathrm{orient}} = \sum_{i=1}^{N} \lambda_0 \sin^2 \psi_i \quad (2)$$

where $\lambda_0$ is the coupling parameter which has the dimension of an energy, and $\psi_i$ is the angle formed by the axis of symmetry of

 

particle $i$ in an instantaneous configuration and the corresponding axis in the reference configuration. The free energy contribution due to the orientational field was evaluated using MC integration.

Typically between 15 and 20 values of the coupling parameter $\lambda^* = \lambda_t/k_BT/(2\sigma)^2 = \lambda_0/k_BT$ were used to perform the integration from the real system to the Einstein crystal. The value of the integrand at each of these intermediate values of $\lambda^*$ was evaluated by means of an *NVT* simulation exerted over about 50 000 cycles for equilibration plus another 200 000 MC cycles for taking averages. For more details on free energy calculations using the Einstein molecule method see ref. 33 and 37. Some values of the free energy obtained using this method are given in the Appendix.

The free energy of solids is known to exhibit a system size dependence and, therefore, a rigorous calculation would require the evaluation of the free energy at different system sizes and an extrapolation of this quantity to infinite system size. However, previous work has shown that for the sizes considered in this work ($N \gtrsim 500$) finite size effects are usually small[33] and for that reason we did not explore this issue further.

### C. Thermodynamic integration

For the fluid phase the free energy was evaluated by thermodynamic integration using as a reference system either the ideal gas (*i.e.*, integrating from very low densities)[37] or the hard-sphere fluid[23] (*i.e.*, integrating from very high temperatures at which the IPCs considered in this work behave virtually as hard spheres, for which the free energy was obtained using the equation of state of Kolafa[39]). As we will see later, our model system exhibits liquid–vapour separation and, therefore, integration from the low density limit must be performed at supercritical temperatures to avoid crossing the phase separation region. Both integration routes were used at different thermodynamic conditions obtaining good agreement between them (see details in the Appendix).

Once the free energy of a particular phase is known at a given thermodynamic state, the free energy at another point can be obtained by thermodynamic integration along an isotherm or along an isobar. The coexistence point between competing phases is then estimated by imposing the condition of thermodynamic equilibrium, *i.e.* two phases are at equilibrium when they exhibit the same chemical potential at the same temperature and at the same pressure.[37]

Starting from one known coexistence point, the entire coexistence line can be traced by using the Gibbs–Duhem method,[40,41] which consists of numerically integrating the Clausius–Clapeyron equation.

Throughout this work, we have regularly performed thermodynamic consistency checks (*i.e.* comparison of the free energy at a given state point obtained *via* different thermodynamic routes) in an effort to avoid errors in the evaluation of the phase diagram (see the Appendix for further details).

### D. Direct coexistence method

As mentioned before, in the layered structure particles are oriented with their symmetry axes parallel to the planes, exposing the equatorial region between planes. As a consequence, at moderate pressures the distance between the layers is relatively large because the system tries to minimize the energy penalty arising from equatorial–equatorial contacts between adjacent layers, and at finite temperatures layers are almost free to slide with respect to each other. This complicates the evaluation of the free energy using the usual Einstein crystal or Einstein molecule methods because it leads to a quasi-divergence in the integrand that needs to be evaluated in going from this structure to the Einstein reference crystal.

This problem was avoided by using the direct coexistence method[42,43] which has been successfully used in the past to calculate the melting point of many systems, including water,[44] hard-spheres, and patchy particle solids[45] or quasicrystals,[46] just to mention a few examples. This method consists of building a simulation box in which the solid is in contact with the fluid phase. Then the coexistence point can be simply estimated by, for example, fixing the temperature and monitoring the evolution of the fluid–layered interface at different pressures. If the actual pressure is higher than the coexistence pressure, the layered structure will grow at the cost of the liquid, whereas if it is lower than the coexistence pressure the layered structure will melt. For this particular structure the kinetics of the growth and the melting of the crystal is much faster when the fluid–layered structure interface is perpendicular to the layers: for this orientation of the interface particles at the edges of the layers expose the polar patches to the melt, allowing the formation of bonds with particles from the fluid during the growth of the layers at pressures above coexistence, or acting as lattice defects within the close-packed layers that promote the melting at pressures below coexistence.

Initially the system contained 480 particles in the parallel layers phase plus another 480 particles in the fluid phase, *i.e.* the total number of particles was $N = 960$. Snapshots of the starting and the final configurations at $T^* = 0.159$ for three different pressures are shown in Fig. 3. The evolution of the interface at these thermodynamic conditions was investigated by performing *NpT* simulations in which the three edges of the box were allowed to change independently. As our system contains an interface, the pressure is in fact an anisotropic tensor and, therefore, strictly speaking, only the size of the edge perpendicular to the interface should be allowed to vary (corresponding to a $Np_NT$ ensemble[47]). However, it is usually preferable to allow changes in the three edges, because this ensures that the solid is relaxed to its equilibrium structure. The error introduced by the presence of the interface in the *NpT* simulations is small provided that the edge of the simulation box perpendicular to the interface is much larger than the edges parallel to it.[48] We observe complete melting at $p^* = 1.40$ and complete crystallization at $p^* = 1.79$. However, at $p^* = 1.59$ the interface remains stable over long times ($\sim 10^7$ MC cycles), evidencing that this pressure is close to the coexistence one. By performing simulations on a finer grid of pressures, we were able to bracket the coexistence point within the interval $1.591 < p^* < 1.600$, taking $p^* = 1.595$ as the coexistence pressure. Note that the kinetics of the system becomes extremely slow as the temperature is lowered: using this method at $T^* = 0.127$ we

could only bracket the coexistence pressure within the interval $0.464 < p^* < 0.637$, the interface remaining quite stable within this range for very long simulation times ($\sim 10^7$ MC cycles).

Once the melting point has been obtained by the direct coexistence method, the free energy of the layered structure can be estimated by resorting to the condition of thermodynamic equilibrium that implies that two phases are in equilibrium at a given pressure and temperature if they have the same chemical potential. Therefore, the free energy of the layered structure at the melting point can be estimated by evaluating the free energy of the fluid phase at that point.

The coexistence of the FCC plastic crystal with the fluid phase was also evaluated using this method. In this case the initial simulation box contained 500 particles in the solid phase and another 500 particles in the fluid phase. For simplicity the interface was built such that the FCC plastic crystal exposed the (0, 0, 1) planes to the fluid phase. In this case the kinetics of the growth or melting of the crystal was quite fast (usually the interface clearly evolves to the crystal or the melt within $10^5$ to $10^6$ MC cycles) allowing us to estimate the melting point using relatively short simulations and thus we did not deem necessary to explore other orientations of the FCC plastic crystal to the interface.

### E. Liquid–vapour separation

The liquid–vapour coexistence line was evaluated using a combination of grand-canonical Monte Carlo (GCMC) and Gibbs ensemble simulations. A first rough estimate of the critical point was obtained by finding a subcritical thermodynamic state (specified by the chemical potential $\mu$ and $T$) for which the system exhibits large fluctuations in density and energy, transitioning between the liquid and vapour phases with relatively high frequency. At this thermodynamic state, we evaluated the probability distribution of the order parameter $M \sim \rho + su$,[49] $s$ being the mixing parameter, $\rho$ the number density and $u$ the energy per particle, that showed a doubled peaked shape close to the critical point. The precise location of the critical point was then obtained by using histogram reweighting[49] and searching for the thermodynamic conditions and the value of the $s$ parameter for which the probability distribution of the order parameter $M$ matches that of the 3D Ising model.

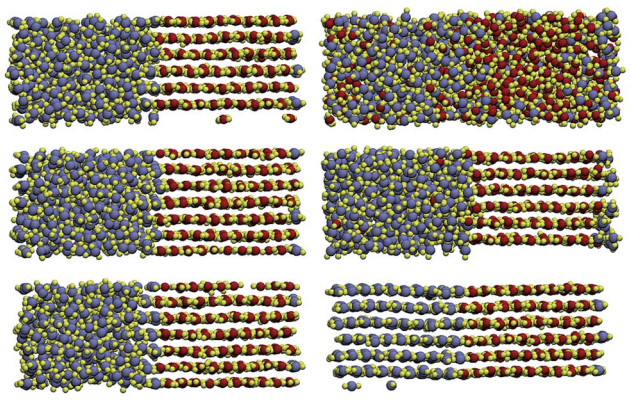

Fig. 3 Initial (left column) and final configurations (right column) obtained with the direct coexistence method for the liquid–parallel layer interface at $T^* = 0.159$ and at pressures below coexistence ($p^* = 1.40$, top panel), near the coexistence point ($p^* = 1.59$, middle panel) and above the coexistence point ($p^* = 1.79$, bottom panel). The particles that are initially in the fluid state are coloured in blue whereas those initially belonging to the parallel layers are coloured in red. In both cases the two patches at the poles of the particles are shown in yellow.

## IV. Results

The calculated phase diagram in the $p$–$T$ representation is shown in the top panel of Fig. 4. The two ordered structures

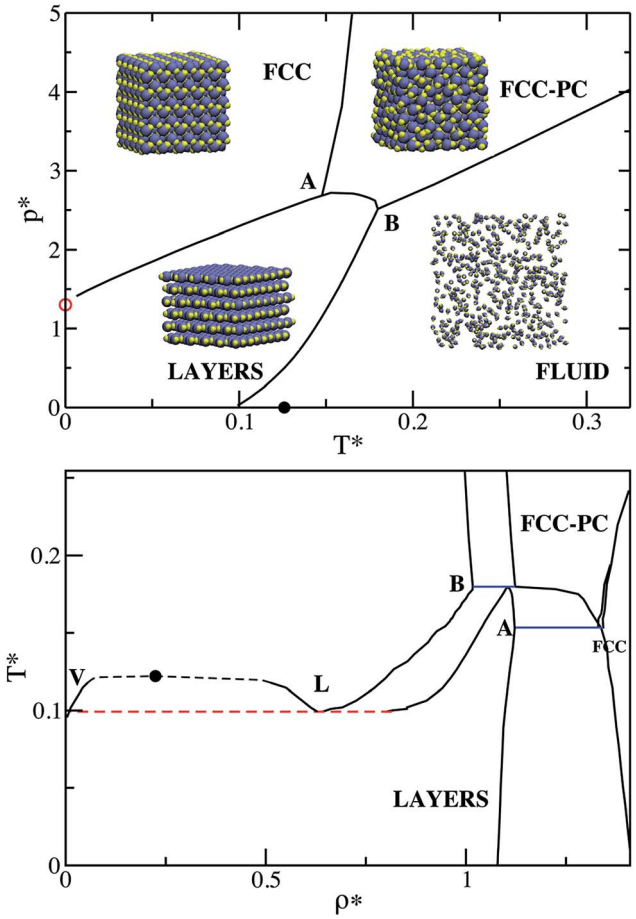


Fig. 4 Phase diagram in the $p$–$T$ (top) and the $T$–$\rho$ (bottom) representations. The coexistence point between the parallel layers and the FCC solid obtained at zero temperature is shown as a red circle in the $p$–$T$ diagram. In the $T$–$\rho$ diagram, the blue horizontal line labelled A signals the triple point in which the layered structure, the FCC plastic crystal and the FCC coexist, whereas the one labelled B signals the triple point between the fluid, the layered structure and the FCC plastic crystal. Each of these lines corresponds to the point labelled with the same letter in the $p$–$T$ diagram. The black dot shows the location of the critical point and the black dashed line is a guide to the eye that connects the highest temperature for which the liquid–vapour coexistence was evaluated using Gibbs ensemble simulations and the critical point. The red dashed line represents the lower limit for which we were able to evaluate either the vapor–liquid or the liquid–layered structure coexistence lines.

predicted as the most stable phases at zero temperature, namely, the parallel layers and the FCC solid, are able to survive over a quite broad range of temperatures. Note that the extrapolation of the coexistence line between these two phases to zero temperature matches the coexistence pressure ($p^* \approx 1.30$) obtained with the evolutionary algorithm (shown in the plot by a red circle), giving us confidence on the reliability of these calculations. Upon increasing the temperature the range of stability of the layered structure increases at the expense of the FCC solid. The layered structure has a higher entropy than the FCC solid which is probably due to a higher vibrational entropy associated with the pronounced vibrations of the particles tilting out of the planes, favouring its stabilization at high temperatures.

This model exhibits a stable vapour–liquid separation that starts at a triple point in which the vapour, the liquid and the layered solid coexist, and ends at a critical point shown as a black dot in Fig. 4. An initial guess of the location of the critical point was obtained by performing GCMC simulations in a cubic box of edge $L = 11$Å. By reweighting the probability distribution of the order parameter $M \sim \rho + su$ for this initial point, we searched for the parameters that better fitted the distribution of $M$ to that of the 3D Ising model. The distribution was symmetric and the better match was achieved for a nearly zero mixing parameter, $s = 0$, and for $T_c^* = 0.122$ and $\rho_c^* = 0.235$. As we are more interested in the ordered phases, we have not accurately evaluated the pressure at the critical point. However, a rough estimation can be obtained from the equation of state along the critical temperature that suggests that the critical pressure is below $p^* \lesssim 0.2$. The precise location of the triple point could not be estimated because it occurs at very low temperatures ($T^* \sim 0.1$) where the equilibration of the liquid is prohibitively slow. Below the triple point the layered structure coexists with a gas of particles whereas above this temperature it coexists with the liquid.

The FCC solid above a given temperature transforms *via* a first order phase transition into a plastic crystal in which the particles occupy the sites of an FCC lattice but have sufficient kinetic energy to rotate almost freely. This transition occurs at temperatures at which the layered structure is still thermodynamically stable, thus resulting in a triple point at which the layered structure, the FCC solid and the FCC plastic crystal coexist (located at $T^* = 0.148$ and $p^* = 2.683$ and labeled A in Fig. 4). By increasing the temperature even further the FCC plastic crystal melts, giving rise to another triple point at which the liquid, the layered structure and the FCC plastic crystal coexist (located at $T^* = 0.178$ and $p^* = 2.51$ and labeled B in Fig. 4).

The $T$–$\rho$ phase diagram is shown in the bottom panel of Fig. 4. Starting the discussion with the parallel layers, it can be seen that the range of densities at which this phase is thermodynamically stable increases as the temperature is lowered: this is related to the fact that the corresponding coexistence pressure with the liquid decreases as the temperature goes down, thus allowing the layered structure, which exhibits only weak interactions between the neighbouring parallel layers, to expand to lower densities by increasing the inter-layer distance. Due to the difficulty of equilibrating the system at low temperatures, we could not evaluate accurately neither the liquid–vapour nor the liquid–parallel layer coexistence lines down to the triple point; thus we cannot provide reliable estimates of the densities of those three phases at the triple point. The dotted red line (at $T^* \approx 0.1$) in the lower panel of Fig. 4 marks the lower limit for which reliable data of the coexistence lines can be provided. Below the triple point, a gas of particles is in coexistence with the layered structure. We attempted to estimate the coexistence between those phases at $T^* = 0.095$ (*i.e.*, a temperature most likely below the triple point). However, at such low temperatures, it is extremely expensive to obtain well converged averages for both the fluid and the layered structure. For example, for the layered structure, an inspection of the configurations reveals that at these low pressure values there is quite a high probability that the system evolves to vanishing densities by increasing the inter-layer distance (thus leading to an increase in entropy) while preserving a close-packed configuration within each layer (thus preserving a quite low energy). Nonetheless, we also observed that in some of the analysed configurations the inter-layer distance does not extend beyond the interaction range, due to the formation of temporary inter-layer bonds. These bonds between the layers can only form when the bonds within the layers are slightly distorted (*i.e.* when the particles tilt out of their plane) as a result of the thermal vibrations of the particles in the system. The formation of such attractive bonds does not invariably lead to a lower total energy: our simulations provide very similar average energies both in the presence and in the absence of inter-layer bonds (the first case being lower with respect to the second by about 0.1%, within the statistical uncertainty). It might be that in the thermodynamic limit the many weak inter-layer bonds due to kinetic vibrations are sufficient to stabilise the inter-layer distance within the particle interaction range, the lowering of the energy would compensate the entropy loss, thus favouring more packed layered structures. On the other hand, at zero temperature the layered structure is the most stable phase down to $p^* = 0$ and at zero temperature and pressure there is a degeneracy between all parallel layered structures with any distance between the layers larger than the interaction range of the IPCs. Thus it also seems plausible that at very low temperature and pressure values, less packed layered configurations could be favoured, since distortions of intra-layer bonds due to thermal fluctuations become less and less favourable as soon as the temperature approaches zero. Further and more extensive (and thus more expensive) studies would be needed to clarify the behaviour of the system in such a region of the phase diagram. Since thermodynamic integration becomes prohibitively difficult in this regime, we assume that the coexistence pressure will shift to lower values as the temperature is decreased, since the entropic contribution to the free energy (that favours the gas of particles) becomes less relevant as we approach zero temperature.

By increasing the density, the layered structure transforms into a close-packed FCC structure. As mentioned before, when the temperature is increased, this FCC solid becomes a plastic crystal. The orientational first order transition of the FCC lattice

is accompanied by small discontinuities either in the density or in the energy and the transition occurs with very little hysteresis of these two quantities (see more details in the Appendix). Therefore the coexistence line between the FCC crystal and plastic crystal phases can be obtained by simply heating and cooling the system at different pressures. By reducing the density, the FCC plastic crystal can coexist with the parallel layers below the triple point B and with the fluid above this point. Curiously, at coexistence, the density of the fluid and of the FCC plastic crystal decreases slightly as temperature increases. This is probably due to the fact that the energy of the fluid is lower than that of the FCC plastic at coexistence, because particles in the fluid locally arrange to avoid repulsive equatorial–equatorial contacts.

# V. Outlook and conclusions

In summary, in this work we have evaluated the equilibrium phase diagram of moderately charged IPCs at low screening. At these conditions the IPC model forms a laminar structure in which the particles within each layer are arranged in a close-packed triangular lattice, while the inter-layer interaction is rather weak.

The relatively low energy in combination with a high entropy stabilizes this structure over a wide range of thermodynamic conditions. At high pressures the layered structure transforms into a close packed FCC lattice, which, in turn, becomes a plastic FCC crystal at high temperatures. In addition, this model exhibits a stable liquid–vapour phase separation.

As mentioned in the Introduction, previous simulation studies of simple models had already reported the formation of layered structures. For example it has been found that one-patch particles with a 40% surface coverage can assemble in double layers.[25] Interestingly, spherical particles with a number of sticky patches distributed all over the particle surface are also able to form single layers, mimicking the behaviour of some proteins and inorganic compounds.[21] Probably due to the high computational cost, none of these studies addressed the thermodynamic stability of these layered structures. Romano *et al.*[23] tried to study the stability of a layered structure formed by three-patch colloids with the patches distributed along the equator and forming an angle of 120° between each other. However, in this case, the layered structure was mechanically stable only at very low temperatures, at which obtaining well converged results for the fluid was very computationally expensive; thus, it was not possible to determine whether the layered structure was thermodynamically stable or not.[23] The stabilization of a stacking of layers has also been observed for a system of charged colloids with a dielectric mismatch with the solvent in an external biaxial field.[22] These particles assembled into a stack of layers very similar to the IPC particles studied in the present work, the particles arranged in a fairly compact triangular lattice within each plane with the inter-layer distance being relatively large due to the repulsion between planes.

For future work, it will be interesting to study how the different model parameters (interaction range, patch opening angle, and energy strength constants) affect the stability of the lamellar structure. Intuitively one would think that this phase is stabilized by moderately increasing the size of the patches (thus lowering the energy within the parallel layers). We can also extrapolate from zero-temperature investigations[27] that a large change imbalance between the core of the particles and the patches favours the formation of the layered structure. The reason is that a large charge imbalance leads to stronger patch–patch or equatorial–equatorial repulsions that cannot be avoided in the FCC structure, whereas in the parallel layers there are almost no patch–patch interactions and the equatorial–equatorial repulsion can be minimized by increasing the lateral distance between the planes. Thus, a large charge imbalance increases considerably the energy of the FCC crystal, but probably not so much that of the layered structure, thus stabilizing this structure with respect to the FCC solid. Finally the layered structure might also be stabilized with respect to the FCC crystal for larger interaction ranges; this could possibly lead to a higher energy for the FCC lattice but again most likely not for the layered structure, because, as mentioned before, repulsive equatorial–equatorial interactions in this latter structure can be relaxed by simply increasing the inter-planar distance. If this guess of the effect of the range turns out to be valid, this is at odds with the behaviour of conventional patchy colloids (that have mutually attractive patches on otherwise repulsive cores) for which low density crystals, such as the diamond cubic lattice, are usually stabilized as the range of the interaction decreases due to an increase of the angular vibrational entropy.[45,50] In any case, further calculations are needed to clarify what is the effect of each of the model parameters on the stability of the laminar structure. This issue is particularly interesting as it can help to identify appropriate decorations of the IPC as well as the screening conditions of the solution that favour or hinder the formation of such layered structures. Besides the equilibrium phase diagram, it would be also interesting to explore the kinetics of crystallization of the laminar structure. Also in this case, the study of the effect of each model parameter on the kinetics of crystallization would be specially relevant.

# VI. Appendix

## A. Free energy calculations

The free energy of the fluid phase was evaluated using different thermodynamic paths. At supercritical temperatures, the free energy of the fluid can be obtained by thermodynamic integration from the very low density limit, in which the fluid behaves virtually as an ideal gas:

$$\frac{A(\rho)}{Nk_{\mathrm{B}}T} = \frac{A^{id}(\rho)}{Nk_{\mathrm{B}}T} + \int_0^{\rho} \frac{z(\rho') - 1}{\rho'} \mathrm{d}\rho' \qquad (3)$$

where $A^{id}(\rho)/Nk_{\mathrm{B}}T = \ln(\rho\Lambda^3) - 1$. We took $\Lambda$ equal to the distance unit (*i.e.*, $2\sigma$) as its value does not affect the coexistence properties. If the free energy is required at temperatures lower than the critical point, this route is still valid, but then care must be taken to avoid crossing the vapour–liquid phase transition. This can be done by first integrating along an isotherm above the critical point from the very low density limit using eqn (3), and

 

then integrating along an isochore up to the desired temperature:

$$\frac{A(V,T_2)}{k_B T_2} = \frac{A(V,T_1)}{k_B T_1} - \int_{T_1}^{T_2} \frac{U(T)}{k_B T^2} \mathrm{d}T. \quad (4)$$

However, this integration path is quite long and accumulation of statistical uncertainties can lead to relatively high errors in the final free energies. Therefore, it would be useful to compare the free energies with other methods. An alternative route is to integrate from the high temperature limit, in which the fluid behaves as the hard-sphere fluid. In this case, one can go from the temperature at which we need to evaluate the free energy to infinite temperature (*i.e.*, $\beta \to 0$) by integrating along a $\beta p$ = constant line:[23]

$$\beta_2 \mu(\beta_2, \beta p) = \beta_1 \left( \mu_{HS}(\beta p) + \langle u \rangle_{\beta_1, \beta p} \right) + \int_{\beta_1}^{\beta_2} \langle u(\beta', \beta' p') \rangle_{\beta', \beta' p'} \mathrm{d}\beta', \quad (5)$$

The value of $\beta\mu_{HS}(\beta p)$ was taken from the equation of state of Kolafa.[39]

The two integration paths used for subcritical temperatures are shown in Fig. 5. The free energies obtained integrating from the ideal gas (path I) and from the high density limit (path II) at both supercritical and subcritical temperatures give results that are consistent within the statistical uncertainty (see Table 1).

The thermodynamic consistency of the free energy of the FCC crystal was also checked by evaluating the free energy at two different thermodynamic states. As shown in Table 2 there is very good agreement between the free energy calculated at $T^* = 0.127$ and $p^* = 5.092$ using the Einstein molecule method and the value obtained by thermodynamic integration from the $T^* = 0.127$ and $p^* = 3.183$ state point.

### B. Coexistence points

Some coexistence points for the IPC model are given in Table 3. Again it was checked that the coexistence point evaluated directly at a given temperature was consistent with that obtained using Gibbs–Duhem integration starting from another previously calculated point along the coexistence line (see Table 3).

As mentioned before, the transition between the FCC crystal and the plastic crystal phases occurs with very little hysteresis and, therefore, it can be easily located by simply heating or cooling the system and monitoring the evolution of the density and the energy. As shown in Fig. 6 the change in both the density and the energy becomes lower as pressure increases. We checked that this jump in the energy and density corresponds to an orientational order–disorder transition by monitoring the evolution of the angular distribution probability:

$$P(\theta) = \frac{N(\theta)}{N\Delta\theta} \quad (6)$$

where $N(\theta)$ is the number of molecules for which the instantaneous orientation of the axis of the molecule and its orientation

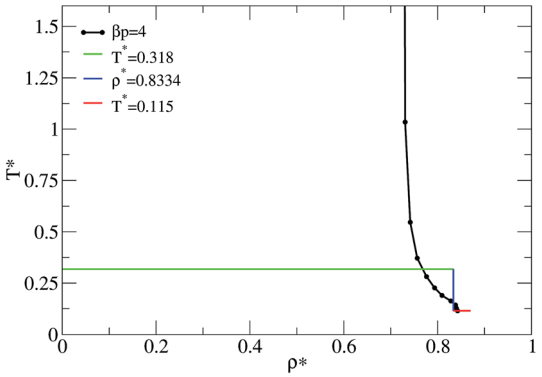


Fig. 5 Two alternative integration paths in the $T^*$–$\rho^*$ phase diagram leading to the free energy along the isotherm $T^* = 0.115$. It is possible to avoid crossing the vapour–liquid transition either by first integrating from the very low density limit (ideal gas) at a supercritical temperature and then performing an integration along an isochore to go to the desired temperature (path I) or by integrating from the high temperature limit (at which the system behaves as the hard-sphere system) along a line in which $\beta p$ = constant (path II).

Table 1 Free energy of the fluid as obtained integrating from the ideal gas (path I) or from the hard-sphere (path II) limits. It can be seen that the relative difference between the free energies obtained with the two methods ($\Delta A/A$) is below 1% either at supercritical ($T^* = 0.318$) and subcritical temperatures ($T^* = 0.115$)

| Path | $T^*$ | $p^*$ | $\rho^*$ | $A/NkT$ | $\Delta A/A$ |
|---|---|---|---|---|---|
| I | 0.318 | 1.273 | 0.743 | 0.931 | |
| II | 0.318 | 1.273 | 0.743 | 0.929 | 0.002 |
| I | 0.115 | 0.509 | 0.839 | −4.176 | |
| II | 0.115 | 0.509 | 0.839 | −4.175 | 0.0002 |

in the reference solid configuration form an angle between $\theta$ and $\theta + \Delta\theta$, and $N$ is the total number of molecules. As shown in Fig. 7, at low temperatures this distribution exhibits a single peak centred at zero degrees (*e.g.* for $T^* = 0.096$). As temperature increases, but still below the transition temperature (*e.g.*, $T^* = 0.127$ and $T^* = 0.159$), the distribution becomes double-peaked, with one peak centred at zero degrees and the other at 180 degrees. At these temperatures, the molecules are still oriented but they have enough kinetic energy to flip between the two energetically equivalent orientations of the molecules. This behaviour is radically different from that observed above the transition ($T^* = 0.223$), for which the angular distribution probability is considerably more uniform. As can be seen in

Table 2 Free energy of the FCC solid obtained using the Einstein molecule (EM) approach. The free energy at the last row was obtained by thermodynamic integration (TI) from the state $T^* = 0.127$ and $p^* = 3.183$

| Method | $T^*$ | $p^*$ | $\rho^*$ | $A/NkT$ | $\Delta A/A$ |
|---|---|---|---|---|---|
| EM | 0.127 | 3.183 | 1.361 | 2.511 | |
| EM | 0.127 | 5.092 | 1.368 | 2.625 | |
| TI | 0.127 | 5.092 | 1.368 | 2.637 | 0.005 |

Table 3 Coexistence points for the IPC model. For the layered structure and the FCC plastic crystal, the location of the phase transition to the fluid phase was estimated by direct coexistence (DC) simulations. As it can be seen, there is good agreement between the coexistence points obtained using DC and those obtained by Gibbs–Duhem (GC) integration starting from a previous coexistence point. The coexistence between the FCC crystal and the parallel layers was obtained by thermodynamic integration, where the free energy of the FCC crystal was calculated by the Einstein molecule method and that of the parallel layers was inferred from the DC simulations (EM + DC)

| Coexisting phases | Method | $T^*$ | $p^*$ |
|---|---|---|---|
| Fluid-layers | DC | 0.159 | 1.60 |
| Fluid-layers | DC | 0.127 | 0.464–0.637 |
| Fluid-layers | GD | 0.127 | 0.51 |
| FCC-layers | EM + DC | 0.127 | 1.57 |
| Fluid-(FCC-PC) | DC | 0.318 | 3.94 |
| Fluid-(FCC-PC) | DC | 0.191 | 2.64 |
| Fluid-(FCC-PC) | GD | 0.191 | 2.60 |

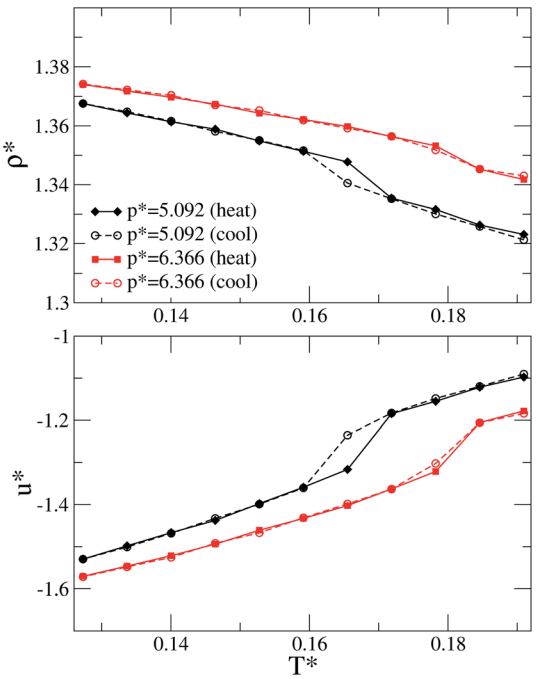


Fig. 6 Evolution of the density and internal energy when heating the FCC crystal or cooling the FCC plastic crystal along the isobars $p^* = 5.092$ and $p^* = 6.366$.

Fig. 7, there are still preferred orientations but the probability that molecules adopt these orientations is only slightly higher than a random orientation. This behaviour of the orientational angle is typical of plastic crystals.

## Acknowledgements

Financial support by the Austrian Science Foundation (FWF) under Project Nos. M1170-N16, V249–N27, P23910-N16, and F41 (SFB ViCoM) is gratefully acknowledged. This work was also funded by Dirección General de Investigación Científica y Técnica under Grant no. FIS2010-15502. One of us (EGN) would like to acknowledge useful discussions with Noé Almarza, Carlos Vega and Jonathan Doye.

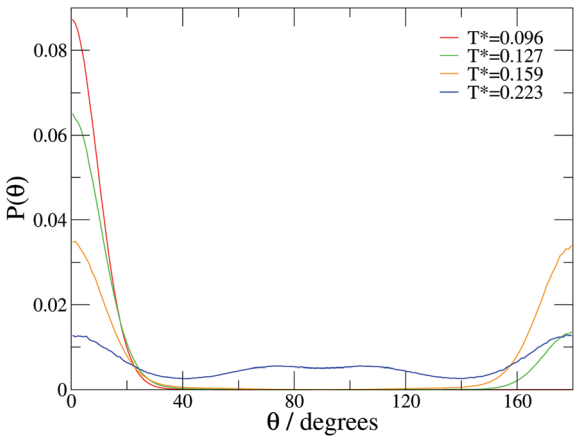


Fig. 7 Orientational distribution probability at different temperatures along the $p^* = 5.092$ isobar. At this pressure, the discontinuity in energy and density occurs at about $T^* = 0.165$. Below this temperature, the distribution shows one or two pronounced peaks at 0 and 180 degrees, respectively, evidencing the orientational order of the molecules, whereas above this temperature a more uniform distribution is observed with only a slight preference for these angles over a random orientation.

## References

1 S. C. Glotzer and M. J. Solomon, Anisotropy of building blocks and their assembly into complex structures, *Nat. Mater.*, 2007, **6**, 557–562.
2 A. B. Pawar and I. Kretzschmar, Fabrication, assembly, and application of patchy particles, *Macromol. Rapid Commun.*, 2010, **31**, 150–168.
3 E. Bianchi, R. Blaak and C. N. Likos, Patchy colloids: state of the art and perspectives, *Phys. Chem. Chem. Phys.*, 2011, **13**, 6397–6410.
4 S. Deka, K. Miszta, D. Dorfs, A. Genovese, G. Bertoni and L. Manna, Octapod-shaped colloidal nanocrystals of Cadmium chalcogenides via "one-pot" cation exchange and seeded growth, *Nano Lett.*, 2010, **10**, 3770–3776.
5 S. Sacanna, W. T. M. Irvine, L. Rossi and D. J. Pine, Lock and key colloids through polymerization-induced buckling of monodisperse silicon oil droplets, *Soft Matter*, 2011, **7**, 1631–1634.
6 L. Rossi, S. Sacanna, W. T. M. Irvine, P. M. Chaikin, D. J. Pineb and A. P. Philipse, Cubic crystals from cubic colloids, *Soft Matter*, 2011, **7**, 4139–4142.
7 Q. Chen, S. C. Bae and S. Granick, Directed self-assembly of a colloidal Kagome lattice, *Nature*, 2011, **469**, 381–384.
8 S. Sacanna, M. Korpics, K. Rodriguez, L. Colón-Meléndez, S.-H. Kim, D. J. Pine and G.-R. Yi, Shaping colloids for self-assembly, *Nat. Commun.*, 2013, **4**, 1688.
9 M. P. Arciniegas, M. R. Kim, J. De Graaf, R. Brescia, S. Marras, K. Miszta, M. Dijkstra, R. van Roij and

L. Manna, Self-assembly of octapod-shaped colloidal nanocrystals into a hexagonal ballerina network embedded in a thin polymer film, *Nano Lett.*, 2014, **14**, 1056–1063.

10 E. Bianchi, G. Kahl and C. N. Likos, Inverse patchy colloids: from microscopic description to mesoscopic coarse-graining, *Soft Matter*, 2011, **7**, 8313–8323.

11 D. A. Christian, A. Tian, W. G. Ellenbroek, I. Levental, K. Rajagopal, P. A. Janmey, A. J. Liu, T. Baumgart and D. E. Discher, Spotted vesicles, striped micelles and Janus assemblies induced by ligand binding, *Nat. Mater.*, 2009, **8**, 843–849.

12 M.-C. Daniel, I. B. Tsvetkova, Z. T. Quinkert, A. Murali, M. De, V. M. Rotello, C. Cheng Kao and B. Dragnea, Role of surface charge density in nanoparticle-templated assembly of Bromvirus protein cages, *ACS Nano*, 2010, **4**, 3853–3860.

13 A. L. Božič and R. Podgornik, Symmetry effects in electrostatic interactions between two arbitrarily charged spherical shells in the Debye-Hückel approximation, *J. Chem. Phys.*, 2013, **138**, 074902.

14 E. Bianchi, C. N. Likos and G. Kahl, Self-assembly of heterogeneously charged particles under confinement, *ACS Nano*, 2013, **7**, 4657–4667.

15 E. Bianchi, G. Kahl and C. N. Likos, Tunable assembly of heterogeneously charged colloids, *Nano Lett.*, 2014, **14**, 3412–3418.

16 Z. Tang, Z. Zhang, Y. Wang, S. C. Glotzer and N. A. Kotov, Self-assembly of CdTe nanocrystals into free-floating sheets, *Science*, 2006, **314**, 274–278.

17 C. Schliehe, B. H. Juarez, M. Pelletier, S. Jander, D. Greshnykh, M. Nagel, A. Meyer, S. Foerster, A. Kornowski, C. Klinke and H. Weller, Ultrathin PbS sheets by two-dimensional oriented attachment, *Science*, 2010, **329**, 550–553.

18 S. Lee, D. T. Lee, J.-H. Ko, W.-J. Kim, J. Joo, S. Jeong, J. A. McGuire, Y.-H. Kim and D. C. Lee, Slow colloidal growth of PbSe nanocrystals for facile morphology and size control, *RSC Adv.*, 2014, **4**, 9842–9850.

19 D. Pum, J. L. Toca-Herrera and U. B. Sleytr, S-layer protein self-assembly, *Int. J. Mol. Sci.*, 2013, **14**, 2484–2501.

20 I. Corni, T. J. Harvey, J. A. Wharton, K. R. Stokes, F. C. Walsh and R. J. K. Wood, A review of experimental techniques to produce a nacre-like structure, *Bioinspiration Biomimetics*, 2012, **7**, 031001.

21 E. Mani, E. Sanz, S. Roy, M. Dijkstra, J. Groenewold and W. K. Kegel, Sheet-like assemblies of spherical particles with point-symmetrical patches, *J. Chem. Phys.*, 2012, **136**, 144706.

22 F. Smallenburg and M. Dijkstra, Phase diagram of colloidal spheres in a biaxial electric or magnetic field, *J. Chem. Phys.*, 2010, **132**, 204508.

23 F. Romano, E. Sanz, P. Tartaglia and F. Sciortino, Phase diagram of trivalent and pentavalent patchy particles, *J. Phys.: Condens. Matter*, 2012, **24**, 064113.

24 T. Vissers, Z. Preisler, F. Smallenburg, M. Dijkstra and F. Sciortino, Predicting crystals of Janus colloids, *J. Chem. Phys.*, 2013, **138**, 164505.

25 G. Munaò, Z. Preisler, T. Vissers, F. Smallenburg and F. Sciortino, Cluster formation in one-patch colloids: low coverage results, *Soft Matter*, 2013, **9**, 2652–2661.

26 The energy constants resulting from the mapping procedure for the chosen microscopic parameters are $u_{PP} \approx 1281.08$, $u_{EE} \approx 55.82$, and $u_{EP} \approx -315.27$ in units of $k_BT$.

27 G. Doppelbauer, Ordered Equilibrium Structures of Patchy Particle Systems, Ph.D. thesis, TU Wien, 2012.

28 G. Doppelbauer, E. G. Noya, E. Bianchi and G. Kahl, Self-assembly scenarios of patchy colloidal particles, *Soft Matter*, 2012, **8**, 7768–7772.

29 G. Doppelbauer, E. G. Noya, E. Bianchi and G. Kahl, Competing ordered structures formed by particles with a regular tetrahedral patch decoration, *J. Phys.: Condens. Matter*, 2012, **24**, 284124.

30 M. Parrinello and A. Rahman, Crystal structure and pair potentials: A molecular-dynamics study, *Phys. Rev. Lett.*, 1980, **45**, 1196.

31 S. Yasonath and C. N. R. Rao, A Monte Carlo study of crystal structure transformations, *Mol. Phys.*, 1985, **54**, 245.

32 E. G. Noya, M. M. Conde and C. Vega, Computing the free energy of molecular solids by the Einstein molecule approach: Ices XIII and XIV, hard-dumbbells and a patchy model of proteins, *J. Chem. Phys.*, 2008, **128**, 154507.

33 C. Vega and E. G. Noya, Revisiting the Frenkel-Ladd method to compute the free energy of solids: the Einstein molecule approach, *J. Chem. Phys.*, 2007, **127**, 154113.

34 D. Frenkel and A. J. C. Ladd, New Monte-Carlo method to compute the free-energy of arbitrary solids. Application to the fcc and hcp phases of hard spheres, *J. Chem. Phys.*, 1984, **81**, 3188–3193.

35 J. M. Polson, E. Trizac, S. Pronk and D. Frenkel, Finite-size corrections to the free energies of crystalline solids, *J. Chem. Phys.*, 2001, **112**, 5539.

36 J. W. Schroer and P. A. Monson, Phase behavior of a hard sphere interaction site model of benzene, *J. Chem. Phys.*, 2000, **112**, 8950.

37 C. Vega, E. Sanz, J. L. F. Abascal and E. G. Noya, Determination of phase diagrams via computer simulation: methodology and applications to water, electrolytes and proteins, *J. Phys.: Condens. Matter*, 2008, **20**, 153101.

38 J. L. Aragonés, E. G. Noya, C. Valeriani and C. Vega, Free energycalculations for molecular solids using GROMACS, *J. Chem. Phys.*, 2013, **139**, 034104.

39 J. Kolafa, Nonanalytical equation of state of the hard sphere fluid, *Phys. Chem. Chem. Phys.*, 2006, **8**, 464–468.

40 D. A. Kofke, Direct evaluation of phase coexistence by molecular simulation via integration along the saturation line, *J. Chem. Phys.*, 1993, **98**, 4149–4162.

41 D. A. Kofke, Gibbs–Duhem integration: A new method for direct evaluation of phase coexistence by molecular simulation, *Mol. Phys.*, 1993, **78**, 1331–1336.

42 A. J. C. Ladd and L. V. Woodcock, Triple-point coexistence properties of the Lennard-Jones system, *Chem. Phys. Lett.*, 1977, **51**, 155.

43 A. J. C. Ladd and L. V. Woodcock, Interfacial and coexistence properties of the Lennard-Jones system at the triple point, *Mol. Phys.*, 1978, **36**, 611.
44 R. G. Fernández, J. L. Abascal and C. Vega, The melting point of ice Ih for common water models calculated from direct coexistence of the solid-liquid interface, *J. Chem. Phys.*, 2006, **124**, 144506.
45 E. G. Noya, C. Vega, J. P. K. Doye and A. A. Louis, The stability of a crystal with diamond structure for patchy particles with tetrahedral symmetry, *J. Chem. Phys.*, 2010, **132**, 234511.
46 J. P. K. Doye, A. A. Louis, I.-C. Lin, L. R. Allen, E. G. Noya, A. W. Wilber, H. Chwan Kok and R. Lyus, Controlling crystallization and its absence: proteins, colloids and patchy models, *Phys. Chem. Chem. Phys.*, 2007, **9**, 2197–2205.
47 D. Frenkel and A. J. C. Ladd, Simulations: The dark side, *Eur. Phys. J. Plus*, 2013, **128**, 10.
48 E. G. Noya, C. Vega and E. de Miguel, Determination of the melting point of hard spheres from direct coexistence simulation methods, *J. Chem. Phys.*, 2008, **128**, 154507.
49 N. Wilding, Simulation studies of fluid critical phenomena, *J. Phys.: Condens. Matter*, 1997, **9**, 585–612.
50 F. Romano, E. Sanz and F. Sciortino, Role of the range in the fluid-crystal coexistence for a patchy particle model, *J. Phys. Chem. B*, 2009, **113**, 15133.